Since January 2020 Elsevier has created a COVID-19 resource centre with free information in English and Mandarin on the novel coronavirus COVID-19. The COVID-19 resource centre is hosted on Elsevier Connect, the company's public news and information website.

Analytica Chimica Acta 1147 (2021) 30–37

Contents lists available at ScienceDirect

Analytica Chimica Acta

journal homepage: www.elsevier.com/locate/aca

3D-printed electrode as a new platform for electrochemical immunosensors for virus detection

Gustavo Martins [a], Jeferson L. Gogola [a], Lucas H. Budni [a], Bruno C. Janegitz [b, *], Luiz H. Marcolino-Junior [a], Márcio F. Bergamini [a, **]

[a] Laboratório de Sensores Eletroquímicos (LabSensE), Departamento de Química, Universidade Federal Do Paraná (UFPR), CP 19032, CEP, 81531-990, Curitiba, PR, Brazil
[b] Departamento de Ciências, Matemática e Educação. Universidade Federal de São Carlos (UFSCar), 13600-970, Araras, SP, Brazil

HIGHLIGHTS

- Commercial 3D conductive filament of polylactic acid (PLA) to construction of immunosensors.
- Sensor construction based on carboxylic group naturally present at filament without any additional pretreatment.
- Immunosensor for diagnosis of Hantavirus disease.
- Feasible, simple, and low-cost alternative strategy to detect viral diseases.

GRAPHICAL ABSTRACT

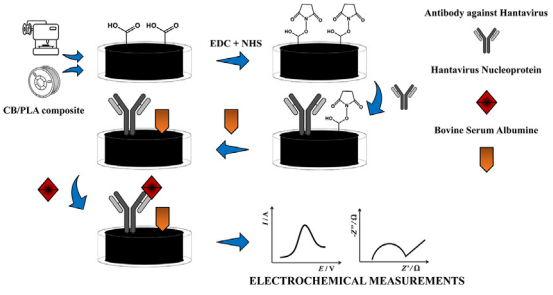

ARTICLE INFO

Article history:
Received 10 July 2020
Received in revised form
20 October 2020
Accepted 7 December 2020
Available online 11 December 2020

Keywords:
3D conductive filament
Immunosensor
Virus detection
Hantavirus araucaria

ABSTRACT

Simple, low-cost, and sensitive new platforms for electrochemical immunosensors for virus detection have been attracted attention due to the recent pandemic caused by a new type of coronavirus (SARS-CoV-2). In the present work, we report for the first time the construction of an immunosensor using a commercial 3D conductive filament of carbon black and polylactic acid (PLA) to detect Hantavirus Araucaria nucleoprotein (Np) as a proof-of-concept. The recognition biomolecule was anchored directly at the filament surface by using *N*-(3-Dimethylaminopropyl)-*N′*-ethylcarbodiimide hydrochloride and *N*-Hydroxysuccinimide (EDC/NHS). Conductive and non-conductive composites of PLA were characterized using thermal gravimetric analysis (TGA), revealing around 30% w/w of carbon in the filament. Morphological features of composites were obtained from SEM and TEM measurements. FTIR measurement revealed that crosslinking agents were covalently bonded at the filament surface. Electrochemical techniques such as cyclic voltammetry (CV) and electrochemical impedance spectroscopy (EIS) were used for the evaluation of each step involved in the construction of the proposed immunosensor. The results showed the potentiality of the device for the quantitative detection of Hantavirus Araucaria nucleoprotein (Np) from 30 μg mL^{-1} to 240 μg mL^{-1} with a limit of detection of 22 μg mL^{-1}. Also, the proposed immunosensor was applied with success for virus detection in 100x diluted human serum samples. Therefore, the PLA conductive filament with carbon black is a simple and excellent platform for immunosensing, which offers naturally carboxylic groups able to anchor covalently biomolecules.

* Corresponding author.
** Corresponding author.
E-mail addresses: brunocj@ufscar.br (B.C. Janegitz), bergamini@ufpr.br (M.F. Bergamini).

https://doi.org/10.1016/j.aca.2020.12.014
0003-2670/

1. Introduction

The detection of viruses has been attracting great attention at this moment due to the recent pandemic of COVID-19 [1]. Therefore, the design of new tools for the diagnostic of this type of pathogen that can be performed quickly and with fewer steps draw higher interest. Sample preparation steps like Polymerase chain reaction (PCR), are often needed but are expensive, complex, require a lot of time and trained personnel. In this context, electrochemical immunosensors are great alternatives for rapid tests with low-cost, which could be useful for clinical trials as well as suitable for the development of point-of-care devices [2,3]. Recently, the development of electrochemical biosensors has shown tendency growth to materials and technologies focused on better performance, simpler arrays, and lower costs essentially focused on the research of point of care devices [4,5]. In light of it, new printing technologies, especially 3D printing, have shown suitable approaches since they can build devices with different layouts, exploring complex geometries and different materials [6–8].

The 3D printing systems based on the extrusion process by using fused deposition modeling (FDM) are the most common [9]. FDM methodology is an additive method, which consists of a layer-by-layer deposition of a semi-molten thermoplastic filament extruded through a fine heated nozzle [10]. The overall characteristics of the process attached to the low-cost, speed, and ease of build guarantees to the 3D printing process by FDM a high versatility and outstanding performance over other conventional manufacturing methods [11]. The FDM printing process has been extensively explored in the construction of sophisticated devices and microfluidic channels, as well as sensors made by other methods, such as electroanalytical microfluidic sample handling systems [12], and even an entire electrochemical cell [13]. There is a huge potential for 3D printing technology in the development of electrochemical sensors based on new conductive filaments and the ability to create complete electrochemical cells of different geometries [14,15]. Although there are 3D printed metal filaments, the most common materials employed in these applications are polylactic acid (PLA), acrylonitrile-butadiene-styrene (ABS), and polyamide (PA) [9,16,17]. Additionally, thermoplastic filaments based on conductive polymer composites have been used in 3D printing for the development of electroanalytical sensors (electrodes) [15,18].

Both systems, 3D printing and electrochemical biosensors working together guarantee agility of construction and assembly, low-cost, portability, and technical simplicity. Such as the glucose biosensor described by Cardoso et., al. [19], which consists of anchoring glucose oxidase directly on the 3D printed electrode, graphene/PLA. Similarly, Marzo et. Al [20]. described a 3D printed biosensor, also based on graphene/PLA, with immobilized horseradish peroxidase (HRP) to create a direct electron transfer enzyme-based biosensor for hydrogen peroxide detection. Most of the 3D printed sensors and biosensors described in the literature are graphene-based, so carbon black/PLA 3D printed electrodes are not so common. However, carbon black (CB) presents interesting characteristics, especially due to its excellent conductivity, electrocatalytic properties, and cost-effectiveness [21,22]. Therefore, CB finds application as a conductive filler material in 3D printing due to the advantages of the material for analyte detection, which is the focus of a few published studies that show the potential of CB as a conductive material on 3D printing filaments applied for electrochemical sensors development [23–25]. Even though the preparation of electrochemical devices using 3D technology has been described, little is known about biosensors based on 3D printed CB/PLA platform, as well as, to the best of our knowledge, there are no reports regarding 3D printed immunosensors.

In this work, we present the first approach of an electrochemical immunosensor based on the direct immobilization of *Hantavirus Araucaria* antibodies onto a commercial 3D conductive filament of carbon black and polylactic acid (PLA) as a proof-of-concept for virus detection. Hantavirus is a single-strained RNA virus, usually found hosted by rats or bats, but represents a higher threat to human beings [26]. The Hantavirus infection in humans commonly results in Hantavirus pulmonary syndrome in the Americas, and hemorrhagic fever with renal syndrome over the Eurasia region, with a lethality rate of over 40%, due to the lack of specific treatment [26]. The early and rapid detection of this virus can be very useful for making clinical treatment decisions [27].

2. Materials and methods

2.1. Materials and reagents

All chemicals were analytical or high-purity grade. *N*-(3-Dimethylaminopropyl)-*N*′-ethylcarbodiimidehydrochloride (EDC), *N*-Hydroxysulfosuccinimide sodium salt (NHS), and Potassium Ferricyanide were purchased from Sigma Aldrich. Potassium chloride was purchased from Merck (Brazil). Acetate buffer, 0.10 mol L^{-1} pH 4.5, from Merck (Brazil) was used to perform EDC/NHS reaction. *Hantavirus Araucaria* nucleoprotein (Np) 1.18 mg mL^{-1}, its IgG2B antibody (HAb) 0.4 mg mL^{-1}, bovine serum album (BSA) and VP2 protein (1.2 mg mL^{-1}) from Gumboro Disease were provided by Molecular Virology Laboratory at Carlos Chagas Institute – FIOCRUZ/PR. Commercial 100x diluted human serum from human male AB plasma (hemoglobin <30 mg dL^{-1}) from Sigma-Aldrich, Conductive-polymer composite PLA/carbon black (Proto-pasta®) was purchased from Protoplant.

2.2. Electrochemical measurements

Electrochemical impedance spectroscopy (EIS) and cyclic voltammetry (CV) measurements were performed using a conventional three-electrode cell. The 3D-printed electrode was used as the working electrode, Pt plate as the auxiliary electrode, and Ag/AgCl (3.0 mol L^{-1} KCl) as the reference electrode. Cyclic voltammetry was carried out in the presence of the electrochemical probe 2.0 mmol L^{-1} $K_3[Fe(CN)_6]$, with 0.1 mol L^{-1} KCl as the supporting electrolyte (potential range from −0.40 to 0.60 V, and a scan rate of 25 mV s^{-1}). CV and EIS experiments were carried out in a potentiostat/galvanostat Metrohm AUTOLAB PGSTAT128 N controlled by a computer using the NOVA 2.1 software. EIS was performed in 2.0 mmol L^{-1} $K_3[Fe(CN)_6]$ and 0.1 mol L^{-1} KCl at a frequency range of 0.1 Hz–100 kHz with 10 mV AC amplitude and potential condition equivalent to the $K_3[Fe(CN)_6]$ anodic peak.

2.3. Thermal, morphological and structural characterization

The thermogravimetric analysis (TGA) was performed by a TGA 4000 (PerkinElmer), under synthetic air atmosphere and heating rate of 5 °C min^{-1}, until 800 °C.

Transmission electron microscopy (TEM) images were obtained on JEOL microscopy, model JEM1200. Scan electron microscopy (SEM) images were performed by FEI High-Resolution Scanning Electron Microscope, model Quanta 450, with field emission gun (FEG) electron source, which has a resolution of 1.0 nm. All images were obtained with 10 kV voltage acceleration and secondary electron detectors.

The Infrared spectra were obtained with BOMEN spectrometer, 64 scans from 4000 cm^{-1} to 500 cm^{-1}. Samples were previously homogenized with KBr pastille and dry.

Characterization studies were done on raw materials (PLA, CB and CB/PLA), before any treatment or printing. Such experiments were performed aiming to verify the PLA/carbon black functional groups as well as the EDC/NHS reaction, used to further anchor the antibodies.

2.4. Working electrode preparation

All parts were printed with a 3D grabber i3 printer, from GTMax 3D (Brazil), through an extrusion nozzle with 0.1 mm precision. The working electrode was printed with a circular geometry of 1.0 cm length and 2.85 mm diameter and 100% infill density (Fig. 1). The printing orientation was selected as horizontal, based on previous studies, as well as described in a similar study [28]. The surface area was delimited by 3D printing 1.0 mm of ABS polymer around PLA/carbon black and the electrical contact was made with copper wire. Before use, the electrode surface was smoothed against sandpaper as previously described on other projects [18,29] and submitted to CV in 0.5 mol L^{-1} NaOH, from −1.2 to 1.2 V at 100 mV s^{-1}, aiming to activate its surface.

To evaluate the printing effect on the electrochemical response of the 3D-printed electrode, a pristine PLA/carbon black filament (raw material) using the same geometrical characteristics (1.0 cm length and 2.85 mm diameter) was also evaluated. The surface was delimited by sealing the electrode with a PVC tube around the filament and the electrical contact was done with copper wire. Before its use, the device was also submitted to similar pretreatment as above described. All the prepared electrodes were electrochemically evaluated by CV measurements using $K_3[Fe(CN)_6]$ as a probe. Those with the best results were used for the construction of the proposed immunosensor.

2.5. Construction of the proposed immunosensor

Firstly, for the preparation of the proposed Hantavirus immunosensor, the evaluated electrodes (3D-printed and raw material) were submitted to EDC and NHS reaction. This step was performed by simply immersing the electrode on an EDC and NHS solution, both of 5.0 mmol L^{-1}, in 0.1 mol L^{-1} acetate buffer solution (pH 4.5) under stirring condition. Subsequently, 5.0 μL of a HAb (0.40 mg mL^{-1}) solution was added directly on the electrode surface, followed by incubation with controlled temperature (4 °C for 60 min). After, a drop-casting of 5.0 μL of a 1.00 mg mL^{-1} BSA solution was added to mitigate possible parallel interactions by blockage of the NHS residual sites. The last step was to detect hantavirus nucleoprotein; therefore, Np was added to the immunosensor surface, which was carried out by drop-casting as well. The immunosensor was gently rinsed with deionized water to remove the molecules that did not bound on the electrode surface after each step used in the sensor preparation. After each step of immunosensor construction, EIS and CV measurements were carried out in presence of the $K_3[Fe(CN)_6]$ probe. Detection was performed comparing the values of resistance of charge transfer (R_{ct}) or peak current before and after incubation in presence of Np for EIS and CV measurements, respectively. All the following steps for sensor construction are summarized in Fig. 2.

2.6. Selectivity evaluation and human serum sample analysis

Aiming to simulate a clinical assay and evaluate possible side reactions with other kinds of proteins that are not Hantavirus derivatives, a spiked 100x diluted human serum sample was evaluated. Thus, the commercial serum sample was submitted to a 1:100 dilution, with 0.1 mol L^{-1} PBS (pH 7.4) and so, spiked with Np to reach a final concentration of 0.120 mg mL^{-1}. The serum samples were added to the electrode surface and submitted to the incubation step for 60 min at 4 °C, so washed and the electrochemical measurements were performed. The selectivity of the proposed immunosensor was also tested against VP2 protein from Gumboro disease. Similarly to the serum sample, it was performed two sets of experiments: (I) VP2 (600 μg mL^{-1}) and a (II) mix of Np (590 μg mL^{-1}) and VP2 (600 μg mL^{-1}) was added to the electrode surface by drop-casting. After incubation at 4 °C for 60 min, they were washed and submitted to electrochemical measurements.

3. Results and discussion

3.1. Thermal, morphological, and structural characterization of conductive filament

The proof-of-concept is an interesting and simple way of understanding new platforms that can be applied for different purposes. In this context, once PLA/carbon black is new material on 3D printing and electrochemical sensors construction, the structure and composition were investigated. SEM and TEM representative images are shown in Fig. 3A and B, respectively.

TEM image (Fig. 3A) shows clusters, possibly from the interaction of branched aggregates with, essentially, globular geometry. SEM image (Fig. 3B) shows a similar structure. However, its amorphous structure stands out and repeats throughout the sample, like

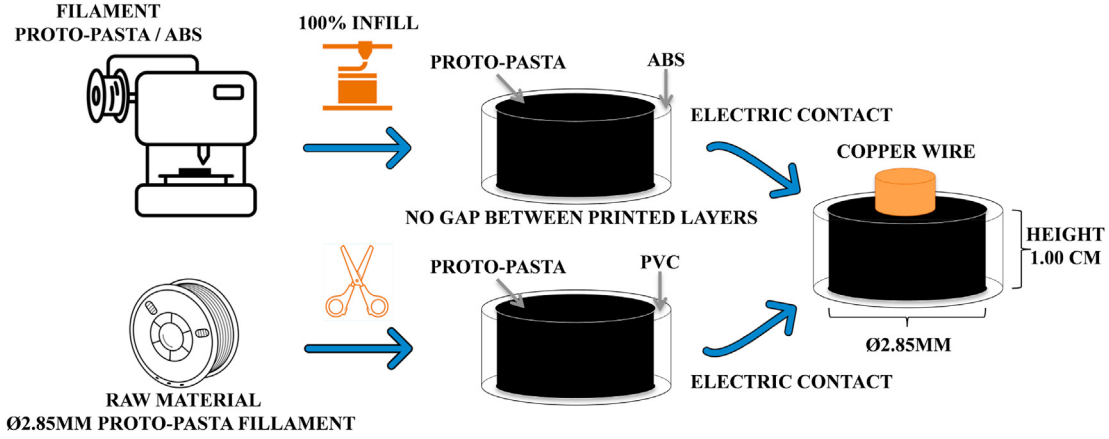

Fig. 1. Buildup of both PLA/carbon black working electrodes.

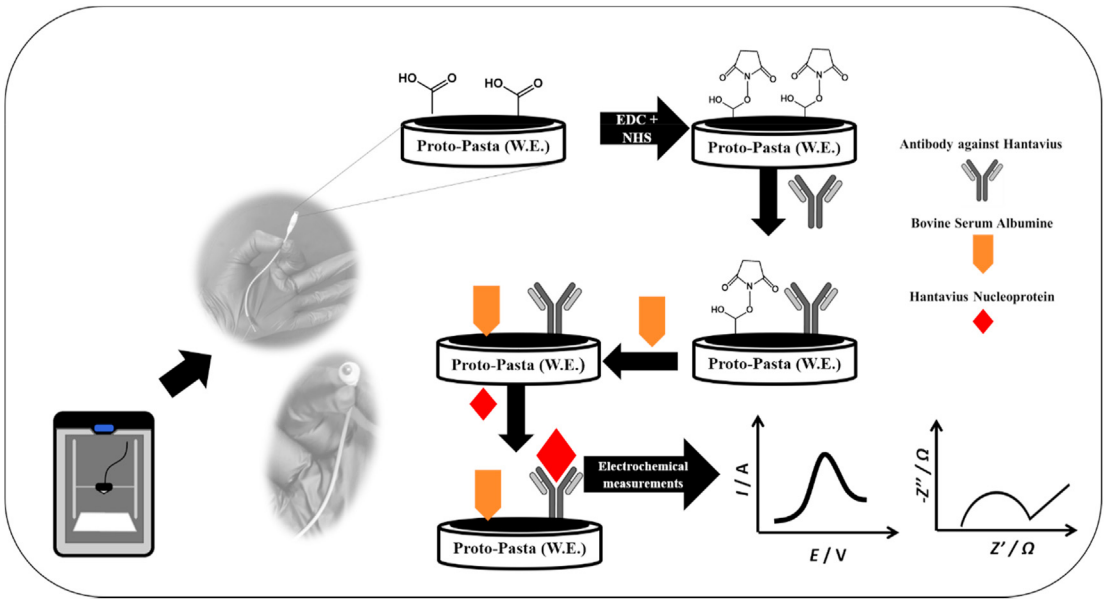

Fig. 2. Immunosensor step by step buildup.

a porous structure, which likely suggests that CB is dispersed throughout the PLA matrix. Fig. S1 shows TEM images of the comparison between standard CB and CB extracted from the PLA matrix. Both samples showed a similar pattern to each other, however, the comparison shows that CB from PLA looks less aggregated, which might be due to residual PLA or solvent effect. PLA/carbon black composite was also characterized by TGA (Fig. 3C). The results show a two-step mass decomposition; the first, at 300 °C, that may be related to the PLA matrix of PLA/carbon black and, subsequently, a thermal decomposition attached to the conductive constituent. On the other hand, standard PLA, TGA analysis, shown only one decomposition process, starting at 300 °C and ending approximately at 380 °C. So, thermal processes above 380 °C may be related to CB decomposition and correspond to 30%

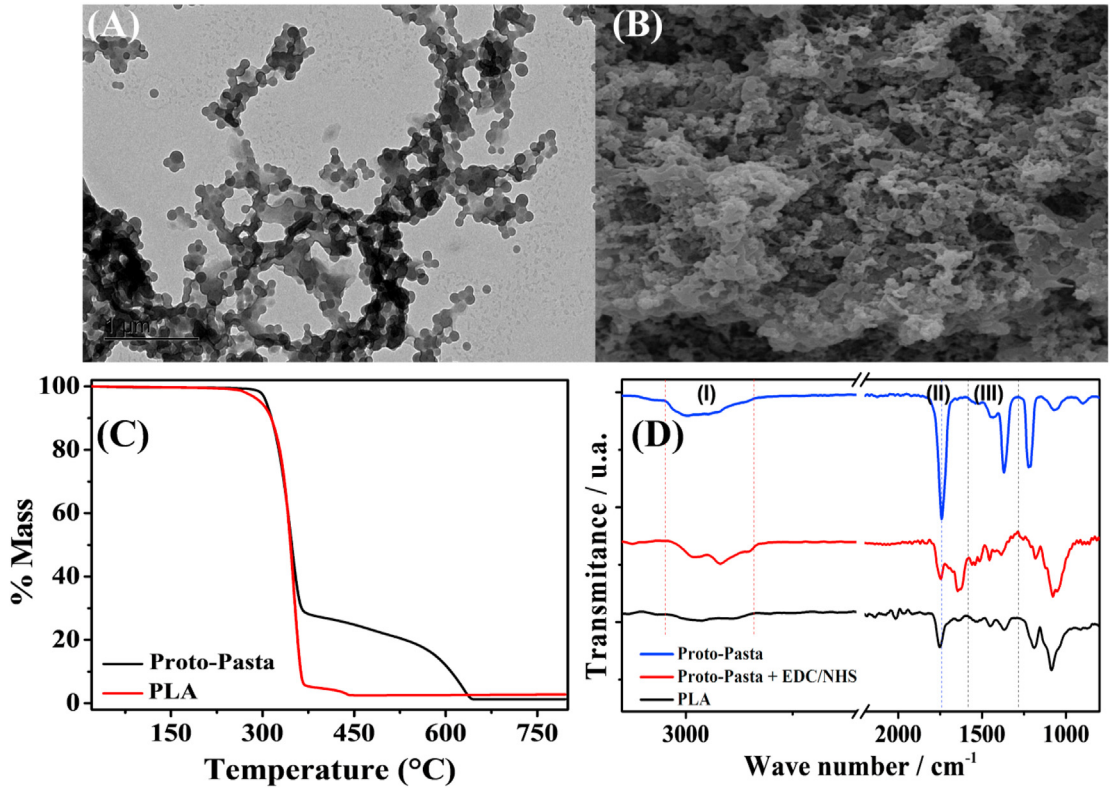

Fig. 3. (A) Representative TEM image obtained to PLA/carbon black with 5 kx. (B) Representative SEM image obtained to PLA/carbon black with 25 kx. (C) PLA/carbon black and PLA thermograms with 5 °C min^{-1} heating rate. (D) FTIR spectras of PLA/carbon black, PLA/carbon black after EDC + NHS reaction and PLA.

of the total decomposed mass, which likely suggests that 30% of the total composite mass is CB.

The surface functional groups were studied by FTIR, as shown in Fig. 3D. FTIR spectra obtained for PLA/carbon black sample presents strong broadband centered in 3000 cm^{-1} (region I), attributed to O–H bond stretch from a carboxylic acid. Another dominant feature can be seen in 1750 cm^{-1} (II), which may be attributed to an asymmetric stretch of C=O, since it is a strong sharp peak centered at 1750 cm^{-1}. The region (III) from 1600 to 1300 cm^{-1} is related to O–H, C–O and C–H bonds. This result has shown the possibility to employ surface carboxylic groups to anchor protein structures exploring EDC – NHS crosslinking reaction. FTIR spectra also show that after EDC/NHS reaction, the 3000 cm^{-1} (I) band splits in two, as well as a significant change in 1750–1300 cm^{-1} band (II and III). Such difference may be related to the bounding of the crosslinking agents onto carboxylic groups, once EDC and NHS present on its structures primary and secondary amines, that stretch over 3000 cm^{-1} region. Also, it overlaps the bands creating the split, as well as the difference in 1750–1300 cm^{-1} band is related to the primary amines deformation frequency, essentially from EDC and NHS [32,33].

The overall analysis of the FTIR spectra has shown that PLA/carbon black 3D-printed electrode surface has presented oxygen functional groups, as well as that EDC – NHS reaction was successfully performed, which allows us to perform the protein anchor by the crosslinking reaction, on further steps.

3.2. Electrochemical characterization of the proposed immunosensor

As mentioned before, Hantavirus was used as a proof-of-concept for virus electrochemical immunosensing [34]. After verified the successful reaction of EDC and NHS on the composite surface, the next steps for biosensor construction were performed.

Before EDC and NHS activation and the immunosensor construction, the electrodes were submitted to a sandpaper polishing and electrochemical activation since the devices showed poor or no clear redox peaks without the treatment. The electrochemical activation process was carried out in a NaOH solution, which removes partially the PLA from the surface by saponification reaction [18]. Thus, the carbon black is more available and consequently improve the electrochemical performance, leading to an enhancement of the signal related to the probe. The steps to anchor the proteins through the crosslinking reaction and to buildup the immunosensor was characterized by CV and EIS measurements, as shown in Fig. 4.

Fig. 4A shows the voltammetric behavior of redox probe $K_3[Fe(CN)_6]$ which blank represents printed electrodes, after electrochemical treatment in NaOH solution (called “bare electrode” from now). After HAb was added by drop-casting of its stock solution, 400 μg mL^{-1}, and anchoring through EDC-NHS crosslinking reaction. Comparing HAb behavior with the bare electrode, it is possible to observe an increase of I_{pa} ($\Delta I = 7.33$ μA), suggesting that HAb was successfully immobilized in the electrode surface. The step consisted of anchoring BSA (1.0 mg mL^{-1}), which was performed to block residual EDC and NHS, taking place on such active sites, causing little insulating effect, reducing the redox probe signal. This behavior granted to the device an increased selectivity since only Np interact with the electrode surface. The last step concerned to detect Np (antigen, 120 μg mL^{-1}), through the formation of the immunocomplex HAb-Np. It is a macromolecule and creates not just an insulating effect, but even a steric impediment, which partially blocks the redox probe interaction with the electrode surface. Therefore, it reflected on the reduction of I_{pa} as shown in Fig. 4 – HAb-BSA-Np, the obtained data is summarized in Fig. 4B. For comparison purposes, all studies performed with the printed device were also carried out using raw PLA/carbon black. Results obtained using not printed electrode are shown in Fig. S2 (A) where a similar electrochemical behavior towards the anchoring processes was observed. However, slight changes in I_{pa} were observed when compared to the printed device. This behavior was probably caused by the intrinsic conductivity of the material and/or an inefficient bounding of the proteins since the lower Np concentration able to be detected was 590 μg mL^{-1}.

The anchoring process performed on the printed electrode (bare) was also evaluated by EIS measurements to confirm the obtained profile and results. The EIS data obtained, Nyquist diagrams – Fig. 4C shows the relation between impedance (resistance to charge transfer) to each step of the immunosensor construction. Therefore, a change to the system resistance indicated a change on the electrode surface, due to the anchoring process of the proteins to build up the device HAb–BSA–Np. Through the fit of the equivalent circuit, R_{ct} was calculated for each step as follows: 2.05 kΩ to the blank (bare PLA/carbon black 3D-printed electrode), 1.00 kΩ after HAb immobilization, which suggests the bounding of HAb. BSA, in turn, increased R_{ct} resistance to 3.63 kΩ, due to the substitution of residual EDC–NHS, since it acts as an insulating molecule. The Np detection consisted of the formation of antibody-antigen (HAb-Np) immunocomplex, such binding leads to an electron transport hindrance, so an increment in R_{ct} value is shown when Np is added, from 3.63 kΩ (HAb-BSA) to 7.39 kΩ (HAb-BSA-Np), suggesting the immunocomplex formation, the obtained data is summarized at Fig. 4D. The raw PLA/carbon black (not printed) device was also evaluated by EIS measurements, again with the same behavior with lower changes when compared to the printed device: 2.72 kΩ to blank electrode, 1.70 kΩ after HAb anchoring, 2.22 kΩ to BSA, and 4.87 kΩ to the Np detection, as shown on Fig. S2(B).

From the above-cited results, we conclude that both studies, CV and EIS, have shown a good correlation between the obtained data to each step of the construction, indicating the success of biomolecules bounding and HAb-Np detection as well.

3.3. Electrochemical response of the immunosensor

Aiming to verify the analytical performance of the proposed immunosensor, the Np concentration range was evaluated through CV of $K_3[Fe(CN)_6]$, by its electrochemical behavior in terms of I_{pa}. Fig. 5A shows the representative CV obtained to the Np detection with concentration ranging from 30 to 580 μg mL^{-1}. The CV data showed a dependence from the Np concentration added and the electrochemical response of the probe, indicating an inert kinetic barrier for the electron-transfer as the Np concentration rises, that is likely related to the antigen-antibody immunocomplex formation, as it acts as an insulating on the device surface [35–37].

As can be seen in Fig. 5B, the I_{pa} values from CV data presented a proportional and linear dependence with the Np concentration in the concentration range of 30 μg mL^{-1} to 240 μg mL^{-1}, that lead to observe a sensitivity of 0.1047 μA μg^{-1} mL and LOD (limit of detection, $3*SD_{blank}$/Slope) equals to 22 μg mL^{-1}. Even though concentration above 240 μg mL^{-1} did not present a linear dependency to the probe (I_{pa}), which is still useful as a qualitative sensor since its application depends on the selectivity to the immunocomplex formation, independent of the concentration.

3.4. Antibody selectivity against VP2 from Gumboro Disease

Before immunosensor application, studies were performed to prove the selectivity of the antibodies against VP2 protein from Gumboro disease. EIS and CV response of the developed

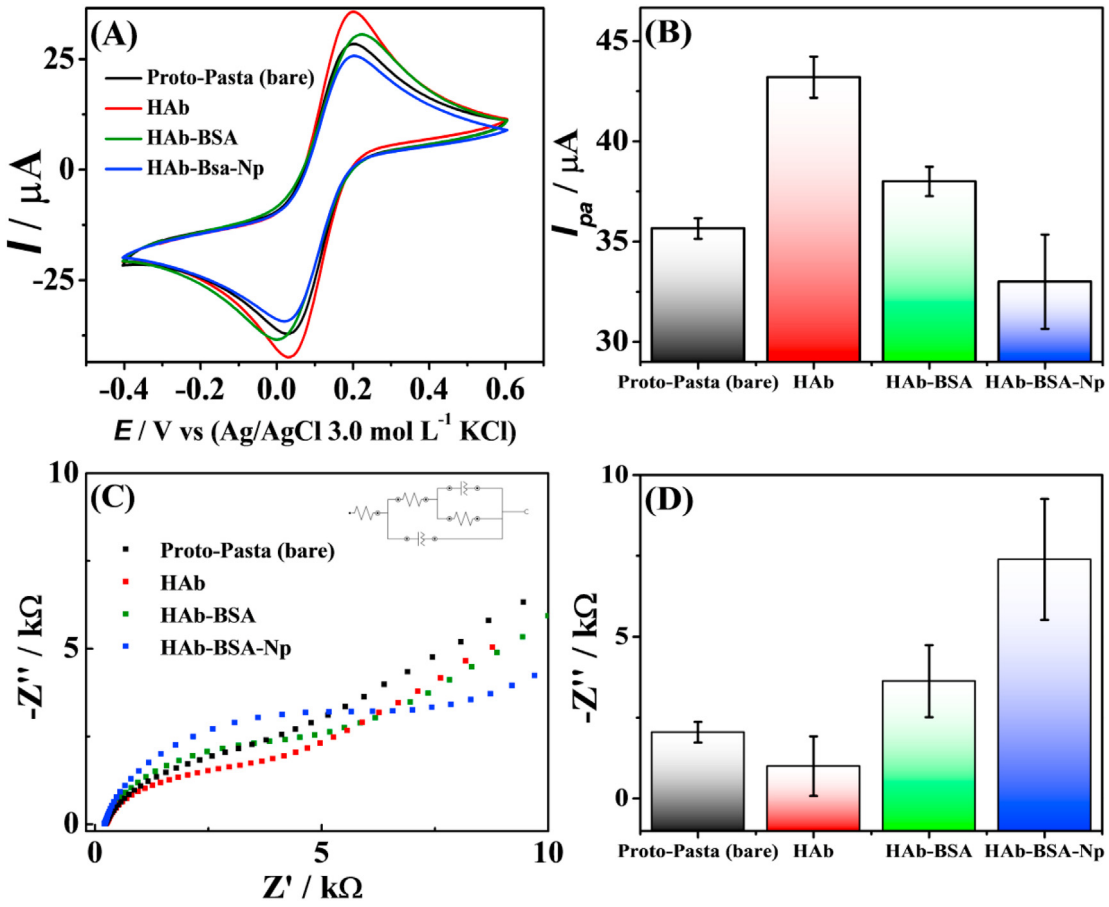

Fig. 4. (A) Cyclic voltammograms of PLA/carbon black 3D-printed electrode, after NaOH treatment, obtained to each step of the immunosensor building, with 2.0 mmol L^{-1} $K_3[Fe(CN)_6]$ and 0.1 mol L^{-1} KCl at a scan rate of 25 mV s^{-1}. (B) Summarized data obtained from CV to each step of anchoring (n = 3, ±SD). (C) Nyquist diagrams obtained from EIS data to PLA/carbon black 3D-printed electrode, after NaOH treatment, on every step of the immunosensor construction, with 2.0 mmol L^{-1} $K_3[Fe(CN)_6]$ and 0.1 mol L^{-1} KCl, 10 mV AC amplitude and anodic peak potential. (D) Summarized data obtained from EIS to each step of anchoring (n = 3, ±SD).

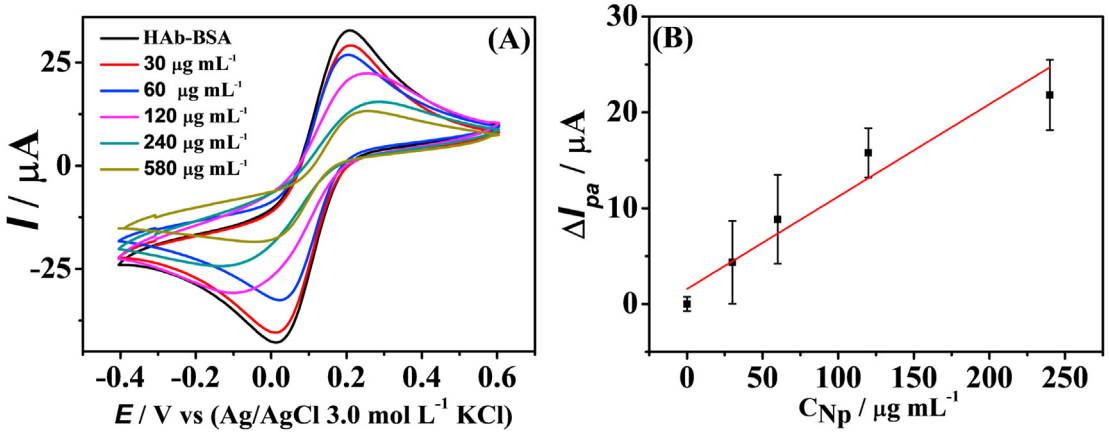

Fig. 5. (A) Cyclic voltammograms of the immunosensor, obtained to different concentrations of Np, with 2.0 mmol L^{-1} $K_3[Fe(CN)_6]$ and 0.1 mol L^{-1} KCl, 25 mV s^{-1}. (B) Calibration curve obtained through probe current peak intensity vs C_{np} (n = 5, ±SD).

imunossensor were tested in the presence of 5.0 µL VP2 protein (600 µg mL^{-1}) which is a potential interferent, once it has a similar basic proteic structure. EIS and CV measurements were recorded using immunosensor in the presence of $K_3[Fe(CN)_6]$, the measurements were performed after incubation (60 min at 4 °C). The experiments were set in the presence of VP2, Np, and a mixture of Np and VP2, and the obtained data is summarized in Fig. S3. In this study, HAb-BSA represents the immunosensor response, HAb-VP2 after drop-casting of 5 µL of VP2 protein (600 µg mL^{-1}), a mixture of Np (590 µg mL^{-1}) and VP2 (600 µg mL^{-1}) was also evaluated. The results of HAb-BSA immunosensor has not shown a significant effect of interferences and had exhibited response only after adding Np (590 µg mL^{-1}). These outcomes suggested that immunosensor has a negligible effect of interferents and the IgG

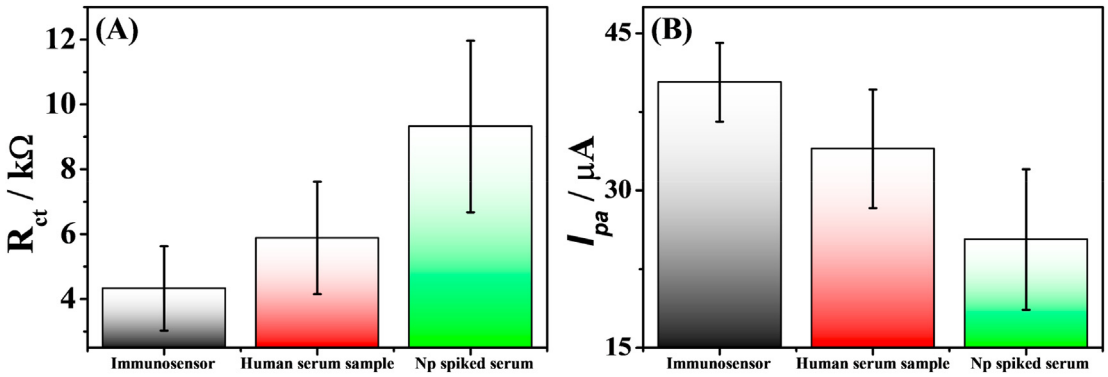

Fig. 6. (A) Serum test and serum fortified with Np obtained through EIS data (n = 5, ±SD). (B) Serum test and serum fortified with Np were obtained through CV data (n = 5, ±SD).

antibody against Hantavirus Araucaria is selective to the Hantavirus Araucaria nucleoprotein only. Thus, the sensor showed a good selectivity allowing, which was used for the detection of Np in the human serum sample.

3.5. Human serum sample analysis

The immunoassay was performed by using a 100x diluted human serum sample spiked with Np (antigen), since this matrix contains proteins and other molecules that may interact by nonspecific binding. For this, the 100x diluted human serum sample solution was added directly on the electrode surface and submitted to incubation step (60 min at 4 °C), after incubation step EIS and CV measurements were recorded in the presence of 2.0 mmol L^{-1} $K_3[Fe(CN)_6]$ as an electrochemical probe. The same set of experiments were performed for the 100x diluted human serum sample spiked with 120 μg mL^{-1} of Np and after incubation step (60 min at 4°) the EIS and CV measurements were performed, the results are summarized in Fig. 6.

The calculated R_{ct} from obtained data has shown a significant increase from 5.88 kΩ (n = 5, SD = 1.52 kΩ) to 9.32 kΩ (n = 5, SD = 2.57 kΩ) in resistance after adding Np to the 100x diluted human serum sample (Fig. 6A). These values are statistically different at a confidence level of 95% ($t_{calculed}$ (2.58) > t_{critic} (2.31)) suggesting the immunocomplex formation under such conditions and an excellent potential analytical for Np detection. By other hand, there was only a slight variation of R_{ct} values from 4.33 kΩ (n = 5, SD = 1.31 kΩ) to 5.88 kΩ ((n = 5, SD = 1.52 kΩ) using 100x diluted human serum in the absence of Np, that did not show significant difference at confidence level of 95% ($t_{calculed}$ (1.73) < t_{critic} (2.31)). This result can be related to the interaction of proteins and other molecules present on the sample matrix with nonspecific binding. Immunocomplex formation leads to a partial blocking of the surface of the device, which has changed significantly the electrochemical behavior of the surface. Thus, as a consequence of the immunocomplex formation, similar results were observed by CV (Fig. 6B), which showed a significant decrease of the peak current from 34.0 μA (SD = 5.46 μA, n = 5) to 25.3 μA (SD = 3.75 μA, n = 5) and a statistical difference between the values after and before incubation step ($t_{calculed}$ (2.92) > t_{critic} (2.31) confidence level of 95%) was observed. As well as there was no significant difference between the immunosensor signal and the 100x diluted human serum ($t_{calculed}$ (1.70) < t_{critic} (2.31) confidence level of 95%). Therefore, EIS and CV techniques have been presented good results demonstrating that both can be used for purpose of diagnosis.

4. Conclusions

3D-printing has gained attention in these last years. They are simple to prepare and filaments with conductive materials provide great alternatives for electrochemical biosensing. On the other hand, virus detection using new methods and tools is extremely important for clinical diagnosis. In this context, this paper reports for the first time, the construction of an immunosensor by using a conductive printable 3D filament with carbon black as the proof-of-concept for Hantavirus detection. The sensor preparation was performed using EDC/NHS combined with carboxylic groups naturally present at the surface of the filament. It was verified that surface properties, as well as oxygen groups, have shown suitable for applying on crosslinking reactions and protein anchoring by covalent bond formation. Also, the proposed device has been responsive and selective to 100x diluted human serum samples. Therefore, the proposed immunosensor platform can be extended for other electrochemical biosensing for clinical diagnosis.

CRediT authorship contribution statement

Gustavo Martins: Conceptualization, Writing - original draft, Writing - review & editing, Formal analysis, Investigation, Data curation, Methodology. **Jeferson L. Gogola:** Conceptualization, Methodology, Writing - original draft, Writing - review & editing, Formal analysis, Investigation, Data curation. **Lucas H. Budni:** Conceptualization, Writing - original draft, Writing - review & editing. **Bruno C. Janegitz:** Conceptualization, Writing - original draft, Writing - review & editing. **Luiz H. Marcolino-Junior:** Conceptualization, Methodology, Writing - original draft, Writing - review & editing, Resources, Supervision, Project administration, Funding acquisition. **Márcio F. Bergamini:** Conceptualization, Methodology, Writing - original draft, Writing - review & editing, Resources, Supervision, Project administration, Funding acquisition.

Declaration of competing interest

The authors declare that they have no known competing financial interests or personal relationships that could have appeared to influence the work reported in this paper.

Acknowledgments

The authors acknowledge the financial support by CNPq (408309/2018-0, 402943/2016-3) and CAPES (88887.504861/2020–00). This study was financed in part by the Coordenação de Aperfeiçoamento de Pessoal de Nível Superior – Brasil (CAPES) –

Finance Code 001, NENNAM (PRONEX, Fund. Araucária/CNPq) and the Molecular Virology Laboratory at Carlos Chagas Institute – FIOCRUZ/PR.

Appendix A. Supplementary data

Supplementary data to this article can be found online at https://doi.org/10.1016/j.aca.2020.12.014.

References

[1] C. Wu, X. Chen, Y. Cai, J. Xia, X. Zhou, S. Xu, H. Huang, L. Zhang, X. Zhou, C. Du, Y. Zhang, J. Song, S. Wang, Y. Chao, Z. Yang, J. Xu, X. Zhou, D. Chen, W. Xiong, L. Xu, F. Zhou, J. Jiang, C. Bai, J. Zheng, Y. Song, Risk factors associated with acute respiratory distress syndrome and death in patients with coronavirus disease 2019 pneumonia in Wuhan, China, JAMA Intern. Med. (2020) 1–10, https://doi.org/10.1001/jamainternmed.2020.0994.

[2] Y. Wang, J. Luo, J. Liu, X. Li, Z. Kong, H. Jin, X. Cai, Electrochemical integrated paper-based immunosensor modified with multi-walled carbon nanotubes nanocomposites for point-of-care testing of 17β-estradiol, Biosens. Bioelectron. 107 (2018) 47–53, https://doi.org/10.1016/j.bios.2018.02.012.

[3] E.K.G. Trindade, R.F. Dutra, A label-free and reagentless immunoelectrode for antibodies against hepatitis B core antigen (anti-HBc) detection, Colloids Surf. B Biointerfaces 172 (2018) 272–279, https://doi.org/10.1016/j.colsurfb.2018.08.050.

[4] E.K.G. Trindade, R.F. Dutra, Point-of-Care electrochemical immunosensors applied to diagnostic in health colloids and surfaces B : biointerfaces A label-free and reagentless immunoelectrode for antibodies against hepatitis B core antigen (anti-HBc) detection, Colloids Surf. B Biointerfaces 172 (2018) 272–279, https://doi.org/10.1016/j.colsurfb.2018.08.050.

[5] Y. Wan, Y. Su, X. Zhu, G. Liu, C. Fan, Development of electrochemical immunosensors towards point of care diagnostics, Biosens. Bioelectron. 47 (2013) 1–11, https://doi.org/10.1016/j.bios.2013.02.045.

[6] C.L. Manzanares Palenzuela, M. Pumera, (Bio)Analytical chemistry enabled by 3D printing: sensors and biosensors, TrAC Trends Anal. Chem. (Reference Ed.) 103 (2018) 110–118, https://doi.org/10.1016/j.trac.2018.03.016.

[7] T. Han, S. Kundu, A. Nag, Y. Xu, 3D printed sensors for biomedical applications: a review, Sensors 19 (2019), https://doi.org/10.3390/s19071706.

[8] J. Muñoz, M. Pumera, 3D-printed biosensors for electrochemical and optical applications, TrAC Trends Anal. Chem. (Reference Ed.) 128 (2020), https://doi.org/10.1016/j.trac.2020.115933.

[9] A. Ambrosi, M. Pumera, 3D-printing technologies for electrochemical applications, Chem. Soc. Rev. 45 (2016) 2740–2755, https://doi.org/10.1039/c5cs00714c.

[10] A. Melocchi, F. Parietti, G. Loreti, A. Maroni, A. Gazzaniga, L. Zema, 3D printing by fused deposition modeling (FDM) of a swellable/erodible capsular device for oral pulsatile release of drugs, J. Drug Deliv. Sci. Technol. 30 (2015) 360–367, https://doi.org/10.1016/j.jddst.2015.07.016.

[11] H.K. Chan, J. Griffin, J.J. Lim, F. Zeng, A.S.F. Chiu, The impact of 3D Printing Technology on the supply chain: manufacturing and legal perspectives, Int. J. Prod. Econ. 205 (2018) 156–162, https://doi.org/10.1016/j.ijpe.2018.09.009.

[12] E.A. Carneiro, D. Agustini, L.C.S. Figueiredo-Filho, C.E. Banks, L.H. Marcolino-Junior, M.F. Bergamini, 3D-printed microfluidic device based on cotton threads for amperometric estimation of antioxidants in wine samples, Electroanalysis 30 (2018) 101–108, https://doi.org/10.1002/elan.201700579.

[13] G.D. O'Neil, S. Ahmed, K. Halloran, J.N. Janusz, A. Rodríguez, I.M. Terrero Rodríguez, Single-step fabrication of electrochemical flow cells utilizing multi-material 3D printing, Electrochem. Commun. 99 (2019) 56–60, https://doi.org/10.1016/j.elecom.2018.12.006.

[14] H.H. Hamzah, S.A. Shafiee, A. Abdalla, B.A. Patel, 3D printable conductive materials for the fabrication of electrochemical sensors: a mini review, Electrochem. Commun. 96 (2018) 27–31, https://doi.org/10.1016/j.elecom.2018.09.006.

[15] V. Katseli, A. Economou, C. Kokkinos, A novel all-3D-printed cell-on-a-chip device as a useful electroanalytical tool: application to the simultaneous voltammetric determination of caffeine and paracetamol, Talanta 208 (2020) 120388, https://doi.org/10.1016/j.talanta.2019.120388.

[16] N. Bhattacharjee, A. Urrios, S. Kang, A. Folch, The upcoming 3D-printing revolution in microfluidics, Lab Chip 16 (2016) 1720–1742, https://doi.org/10.1039/c6lc00163g.

[17] B. Gross, S.Y. Lockwood, D.M. Spence, Recent advances in analytical chemistry by 3D printing, Anal. Chem. 89 (2017) 57–70, https://doi.org/10.1021/acs.analchem.6b04344.

[18] E.M. Richter, D.P. Rocha, R.M. Cardoso, E.M. Keefe, C.W. Foster, R.A.A. Munoz, C.E. Banks, Complete additively manufactured (3D-printed) electrochemical sensing platform, Anal. Chem. 91 (2019) 12844–12851, https://doi.org/10.1021/acs.analchem.9b02573.

[19] R.M. Cardoso, P.R.L. Silva, A.P. Lima, D.P. Rocha, T.C. Oliveira, T.M. do Prado, E.L. Fava, O. Fatibello-Filho, E.M. Richter, R.A.A. Muñoz, 3D-Printed graphene/polylactic acid electrode for bioanalysis: biosensing of glucose and simultaneous determination of uric acid and nitrite in biological fluids, Sensor. Actuator. B Chem. 307 (2020) 127621, https://doi.org/10.1016/j.snb.2019.127621.

[20] A.M. López Marzo, C.C. Mayorga-Martinez, M. Pumera, 3D-printed graphene direct electron transfer enzyme biosensors, Biosens. Bioelectron. 151 (2020), https://doi.org/10.1016/j.bios.2019.111980.

[21] S. Cinti, F. Arduini, M. Carbone, L. Sansone, I. Cacciotti, D. Moscone, G. Palleschi, Screen-printed electrodes modified with carbon nanomaterials: a comparison among carbon black, carbon nanotubes and graphene, Electroanalysis 27 (2015) 2230–2238, https://doi.org/10.1002/elan.201500168.

[22] F. Arduini, F. Di Nardo, A. Amine, L. Micheli, G. Palleschi, D. Moscone, Carbon black-modified screen-printed electrodes as electroanalytical tools, Electroanalysis 24 (2012) 743–751, https://doi.org/10.1002/elan.201100561.

[23] E. Vaněčková, M. Bouša, Š. Nováková Lachmanová, J. Rathouský, M. Gál, T. Sebechlebská, V. Kolivoška, 3D printed polylactic acid/carbon black electrodes with nearly ideal electrochemical behaviour, J. Electroanal. Chem. 857 (2020) 113745, https://doi.org/10.1016/j.jelechem.2019.113745.

[24] A.F. João, A.L. Squissato, E.M. Richter, R.A.A. Muñoz, Additive-manufactured sensors for biofuel analysis: copper determination in bioethanol using a 3D-printed carbon black/polylactic electrode, Anal. Bioanal. Chem. 412 (2020) 2755–2762, https://doi.org/10.1007/s00216-020-02513-y.

[25] R. Cardoso, S. Castro, J. Stefano, R. Muñoz, Drawing electrochemical sensors using a 3D printing pen, J. Braz. Chem. Soc. 31 (2020) 1764–1770, https://doi.org/10.21577/0103-5053.20200129.

[26] T. Avšič-Županc, A. Saksida, M. Korva, Hantavirus infections, Clin. Microbiol. Infect. 21 (2019), https://doi.org/10.1111/1469-0691.12291 e6–e16.

[27] E. Teeple, J. Collins, S. Shrestha, J. Dennerlein, et al., POC diagnostics: recent devs in a connected age, Physiol. Behav. 176 (2018) 139–148, https://doi.org/10.1016/j.physbeh.2017.03.040.

[28] H.H. Bin Hamzah, O. Keattch, D. Covill, B.A. Patel, The effects of printing orientation on the electrochemical behaviour of 3D printed acrylonitrile butadiene styrene (ABS)/carbon black electrodes, Sci. Rep. 8 (2018) 1–8, https://doi.org/10.1038/s41598-018-27188-5.

[29] S. Kim, S.J. Park, Effect of acid/base treatment to carbon blacks on preparation of carbon-supported platinum nanoclusters, Electrochim. Acta 52 (2007) 3013–3021, https://doi.org/10.1016/j.electacta.2006.09.060.

[32] C. Wang, Q. Yan, H.B. Liu, X.H. Zhou, S.J. Xiao, Different EDC/NHS activation mechanisms between PAA and PMAA brushes and the following amidation reactions, Langmuir 27 (2011) 12058–12068, https://doi.org/10.1021/la202267p.

[33] G. Settanni, J. Zhou, T. Suo, S. Schöttler, K. Landfester, F. Schmid, V. Mailänder, Protein corona composition of poly(ethylene glycol)-and poly (phosphoester)-coated nanoparticles correlates strongly with the amino acid composition of the protein surface, Nanoscale 9 (2017) 2138–2144, https://doi.org/10.1039/c6nr07022a.

[34] G. Martins, J.L. Gogola, F.R. Caetano, C. Kalinke, T.R. Jorge, C.N.D. Santos, M.F. Bergamini, L.H. Marcolino-Junior, Quick electrochemical immunoassay for hantavirus detection based on biochar platform, Talanta 204 (2019) 163–171, https://doi.org/10.1016/j.talanta.2019.05.101.

[35] X.P. Li, G. Ji, Z. Chen, A. Addad, Y. Wu, H.W. Wang, J. Vleugels, J. Van Humbeeck, J.P. Kruth, Selective laser melting of nano-TiB2decorated AlSi10Mg alloy with high fracture strength and ductility, Acta Mater. 129 (2017) 183–193, https://doi.org/10.1016/j.actamat.2017.02.062.

[36] C. Thunkhamrak, P. Chuntib, K. Ounnunkad, P. Banet, P.H. Aubert, G. Saianand, A.I. Gopalan, J. Jakmunee, Highly sensitive voltammetric immunosensor for the detection of prostate specific antigen based on silver nanoprobe assisted graphene oxide modified screen printed carbon electrode, Talanta 208 (2020) 120389, https://doi.org/10.1016/j.talanta.2019.120389.

[37] N. Oliveira, E. Costa-Rama, S. Viswanathan, C. Delerue-Matos, L. Pereira, S. Morais, Label-free voltammetric immunosensor for prostate specific antigen detection, Electroanalysis 30 (2018) 2604–2611, https://doi.org/10.1002/elan.201800417.